Journal of Engineering Science and Technology
Vol. 18, No. 5 (2023) 2352 - 2370

EFFECT OF FLY ASH NANO-PARTICLES IN POLYLACTIC ACID VASCULAR TUBES AND NETWORK ON THE HEALING RESULTS OF REINFORCE CONCRETE FOR SUSTAINABLY

NOOR A. HAMEED*, FARHAD M. OTHMAN, ALAA A. ABDUL-HAMEAD

Department of Materials Engineering, University of Technology, Baghdad, Iraq
*Corresponding Author: Mae.20.101@grad.uotechnology.edu.iq

Abstract

Concrete cracks easily in the tensile zone, which is why the steel reinforcing is used in these areas. Small fractures may still form, allowing liquids and gases to enter the reinforcement and cause it to corrode. Self-healing concrete fixes and closes these tiny fissures, preventing the corrosion from forming. In this study, the potential use of fused deposition modelling (FDM) to create new varieties of vascular networks and tubes from polylactic acid (PLA) has been explored. PLA was printed in three dimensions (3D) that were compared to those of both one- and two-dimensional networks (1D and 2D). The outside diameter was (5.6 mm), and the internal diameter was (4 mm). A volume of 10 ml was used in the whole vascular structures (1D, 2D, and 3D) carrying the healing agents as inorganic sodium silicate liquid and nano-powder (fly ash) made from recycled materials using a planetary ball mill, and subsequently, the prepared tubes were embedded into a concrete beam to introduce self-healing properties. The water-cement ratio (W/C) for all concrete mixtures was (0.6%), and the proportions of concrete mixture were (1:2.16:2.98). The actual self-healing effect was measured regarding the recovery of load-carrying capacity after reloading the repaired specimen by four-point bending, the restored strength was 84% for the specimen with 3D. This also improved durability, compressive strength, and other physical features. The produced pipes may thus be utilized to create innovative concrete that can complete the self-healing and be suited for self-healing bridge applications.

Keywords: Concrete, Durability, Mechanical properties, Nano fly ash powder, Self-healing, Sodium silicate solution, Vascular system.

1. Introduction

Concrete is the most widely used construction material because of its high compressive strength and relatively low cost [1]. Concrete intrinsic brittleness makes cracking unavoidable, creating paths for aggressive chemicals to destroy the reinforcing and weaken the structure [2]. Most of these cracks appear because of their limited tensile strength, creep, excess load, permeability, thermal stress, earthquakes, and so on [3]. An effective substitute for traditional methods of repairing the impairment as well as rehabilitation of the components of concrete is the self-repair mechanism [4, 5], implemented via utilizing various methods autogenously (fiber. SCM) or autonomously (Bacteria, capsule). However, the crack width imposes a limit on the autogenous healing. The crack must be around 200 µm or less [6]. Regarding the autonomous healing, one practical example involved releasing a stored healing agent in small amounts from polymer capsules, glass capsules, ceramic capsules, and ZnO capsules [3, 7-9].

A small quantity of healing agents is provided through capsule-based self-healing, which prevents the repetitive damage repair and the healing of more significant cracks [10]. Vascular systems have the considerable benefit of permitting multiple cycles of cracking and healing, since the healing agent may be continually supplied through the flow networks [11].

Many investigations on the impact of the vascular system in sealing the crack in cementitious material and using recycled materials in concrete have been carried out. Siahkouhi et al. [12] examined the bending performance of self-healing concrete railway sleepers (SHCRS) after strengthening the sleepers using polyurethane (PU) filled glass tubes. The exerted stress rose via (11%) in the seat of rail and (450%) in the sleeper center when the slenderness ratio was reduced. Selvarajoo et al. [13] presented a cyanoacrylate delivery system using PET (polyethylene terephthalate) tube networks integrated into cementitious matrices (CA). Three-point flexural bending measurements on notched prisms without reinforcement were carried out. Wan et al. [14] used dissolvable Polyvinyl Alcohol (PVA) filament to create vascular networks that are wax-coated and embedded in cementitious mortar with epoxy resin as the healing agent. To study the healing efficiency, four-point bending tests and permeability tests were conducted.

Li et al. [10] utilized Murray's circulatory blood volume transfer equation to design and build a biomimetic three-dimensional (3D) PLA vascular network. After the sample being fractured as well as pumped with sodium silicate for 4 weeks, the sample's mechanical characteristics were evaluated using load recovery. Tsangouri et al. [15] used a healing system composed of 3D printed polymer tubes that instantly break upon cracking using healing foam polyurethane (PU). The sealed cracks depicted significant strength and toughness recovery. De Nardi et al. [16] created modified formulations of a cyanoacrylate-based glue that might be used in a vascular self-healing cementitious material. According to the findings, a customized formulation boosted the load recovery by 48% when compared to the top performing original formulation. A new type of binding substance, calcium silicate hydrate, is created by the reaction between sodium silicate, employed in the concrete, and calcium hydroxide, already present in the concrete (C-S-H).

Alghamri et al. [17] treated smart aggregates in self-healing concrete. As a 30% substitution for coarse aggregates, lightweight aggregates coated with sodium silicate and sodium nitrate and encased in polyvinyl alcohol covering was used, the

results depicted that the stiffness and flexural strength recovered significantly after healing. Cruz et al. [18] used a coarse limestone aggregate impregnated with sodium silicate solution and encapsulated with polyvinyl alcohol (PVA) in concrete. The result revealed that the compressive strength improved by up to 50% and the presence of the crystalline phases, C-S-H Calcite and Dolomite, via XRD and SEM. Sajjadi and Madandoust [19] studied the impacts of Fly ash and Steel/Polypropylene fibers on the self-healing capacity of concrete that was examined. The outcomes showed that the (15%) fly ash substitution resulted in (94%) permeability decrease and nearly a complete recovery of secondary tensile strength following the re-curing.

The current study creates a 3D vascular network with improved healing agent spreading coverage, and a vascular network has been created utilizing Polylactic Acid (PLA) as well as 3D printing, and its performance was compared to that of the related (1D) and (2D) networks for the application in the self-healing of concrete. It was illustrated that the structures of PLA have an acceptable interfacial connection for mechanical triggering and a brittle fractural response. They were inserted into concrete prisms and subjected to four-point bending cracking to assess their ability to establish a solid link with the cement matrix experimentally. All systems displayed the first fractures that were between 700 and 900 μm in width. It was demonstrated that the pumped sodium silicate liquid with powdered nano fly ash as a healing agent was successfully transported through the vascular network in each of the three systems for seven to twenty eight days. The actual self-healing effect was elucidated in terms of the recovery of load-carrying ability during the mechanical testing after reloading the specimen by four-point bending. The inquiry could cover more healing agents.

2. Experimental Work

The experimental work contains the following two parts:

(a) Fabrication of vascular tubes and networks by 3D printing

The vascular tubes and networks were fabricated by 3D printing with different designs (1D, 2D, and 3D). The creality CR-10S 3d printer, equipped with a 0.80 mm diameter nozzle, was used to fabricate the vascular. Having a maximum printing dimension of (300 mm X 300 mm X 400 mm), the printer's highest achievable print resolution is (60 μm), and it can reach a maximum print speed of 80 mm/s. Polylactic acid (PLA), bio-degradable thermoplastic aliphatic polyester, is made from renewable resources, like corn or sugarcane. Low Tg (about 60°C) and low elongation at break (10%) characterize the PLA [20]. The hollow tubes have a length of (100 mm), an internal diameter of (4 mm), and an outside diameter of (5.6 mm) with a volume of (30 ml).

The printing parameters of filaments adopted for preparing the fused deposition modelling (FDM) samples are listed in Table 1.

The capacity of the tube and vasculature to safeguard the healing agent and the chemical stability of PLA from the cementitious environment and prevent the agent loss from the pipes before rupture is a factor of utmost significance in creating effective tubes self-healing. Since the interlayer adhesion is good when the pipes are made with FDM, further processing like the painting is unnecessary. It can be seen that there are no gaps between the pipes and the concrete.

Table 1. Configurations of printing parameters for PLA material.

Printing parameters	Configurations
Layer height (mm)	0.1, 0.2, 0.3, 0.4, 0.5
Layer orientation	Upright
Printing temperature (°C)	215
Bed temperature (°C)	60
Diameter of filament (mm)	1.75
Diameter of a nozzle (mm)	0.8
Speed of printing (mm/s)	50 mm/s
Raster angle	45/-45
Travel speed (mm/s)	150 mm/s
Infill	100%

To evaluate the mechanical recovery after breaking and to embed into a concrete cube during the casting, tubes made with each plastic filament were filled with liquid sodium silicate and nano fly ash as a healing agent. The specimens were first preserved in water for 28 days, and then these specimens were cut into two to determine if the healing agents were still viable. Because the healing agent was still liquid, the sodium silicate could be used to enable the self-healing process, see Fig. 1.

(a) Embedded 3D tube in concrete.

(b) Splitting the cube by a diamond circularly saw

(c) Optical microscope showing a good homogeneity between tube and concrete

Fig. 1. The position of vascular tube and the extent of homogeneity with the concrete.

(b)The nano-powder preparation

The nano-powder preparation from fly ash was carried out employing a planetary ball mill with porcelain balls at a rotational speed of 400 rpm for three hours.

3.Used materials

3.1. Cement

In the present investigation, Type (I) regular Portland cement was utilized, the requests of Iraqi Specification (No. 5/1984) [21] and standard ASTM (C150-04) [22] are met by the cement's physical characteristics and the chemical compositions, as shown in Table 2.

3.2. Aggregate

As illustrated in Table 2, the coarse aggregates are round and have an ultimate size of (20 mm), while the fine aggregates are natural sand with an ultimate size of (4.75 mm) from the contemporary Mustafa plant in Karbala. These materials meet the standard ASTM (C33-03) [23] and the Iraqi Standard Specification (No. 45/1984) [24].

3.3. Fly ash

The used class (F) fly ash was within the requests of the American Standard ASTM (C 618-15), as evinced in Table 2 [25].

Table 2. Chemical compositions of the used cement, fly ash, and sodium silicate.

Chemical components %	Fe_2O_3	SO_3	SiO_2	Al_2O_3	CaO	MgO	Alkalies (K_2O, Na_2O_3)	Na_2O	L.O.I	C_3A	C_3S	C_2S	C_4AF	L.S.F
Cement	3.13	2.06	20.07	5.74	62.29	2.32	0.60		1.91	9.92	52.07	17.95	9.52	0.96
Fly Ash	2.67	4.3	55.87	20.82	8	0.34		0.26	5.6					
Sodium Silicate			32-33					13.1-13.7						

3.4. Sodium silicate

The utilized sodium silicate in this work was produced in the United Arab Emirates, and its concentration relied upon the percentage of SiO_2 (32-33wt.%), Na_2O (13.1-13.7wt.%), and H_2O (54 wt. %).

3.5. Proportions of mixture

The highly employed weight ratio (1:2.16:2.98) was used for mixing, with a goal strength of (30 MPa) at four weeks. The combination contains 340 kg of cement, 734.4 kg of sand, and 1013.2 kg of gravel per cubic meter. The ratio of water to cement is 0.6. Nano fly ash powder was added to the healing fluid in the hollow tubes at a rate of 10% to create an autonomous self-healing system presented as the mixture of concrete in Table 3.

In the present work, several specimen shapes were prepared, such as cubes, prisms, and cylinders, to assess the mechanical properties of hardened concrete and quantify the physical attributes and toughness. After 7, 28 and cracked samples returned in air condition for further 28 day for healing, the specimens of cured concrete were tested for compressive strength. According to B.S. (1881-116) standard [26], these tests were defined for cubic samples of 150x150x150 mm^3, beams with the dimensions 500 * 100 * 100 mm^3 were constructed to evaluate the flexural strength of concrete specimens after 7 and 28 days using a four-point flexural machine following the standard ASTM (C78) [27]. A vascular network was incorporated with a unique design (1D, 2D, and 3D). The specimens also had 4 mm smooth metal bars for reinforcement which were spaced 10 mm from the specimen's bottom to prevent the complete splitting during the cracking process. The force was applied to the specimens until the beams, which were positioned on two supports 400 mm apart at the two ends, collapsed. Three cylinders (each measuring 100 * 200 mm) were prepared for the Rapid Chloride Penetration Test at the same ages.

Table 3. Mix proportions of concrete beam compressive strength specimens.

Mix	Nano Fly ash (g)	Sodium silicate liquid (ml)	Tubes with a healing agent(g)	Cement (g)	Fine aggregate (g)	Coarse aggregate (g)	Water (ml)	Number sample
Control	0	0	0	1148.56	2480.8	3422.7	689.1	3
1D tube	1	10	17	1148.56	2480.8	3422.7	689.1	3
2D tube	1	10	17	1148.56	2480.8	3422.7	689.1	3
3D tube	1	10	17	1148.56	2480.8	3422.7	689.1	3

3.6. Inspections and tests

3.6.1. Nano-powder inspections

The SEM test was conducted via Electron Gun Tungsten (Japan) having an accelerating voltage from (200 V) to (30 kV).

The particle size of inspected fly ash powder was conducted in the Nanotechnology and Advanced Research Centre using the device (Model: Brookhaven Nano Brook 90 plus, US), and it was found to be 100 nm.

3.6.2. Physical properties test

According to the standard ASTM (C642-97) [28], dry density, water absorption, and porosity were calculated. In this test, pieces from the crushed concrete specimens utilized in the compressive strength test were used. The following equations were used to determine the results of these tests:

$$\text{Dry density } (\text{g/cm}^3) = \frac{w1}{w2 - w3} \times \rho w \quad (1)$$

$$\text{Absorption of Water} = \frac{w2 - w1}{w1} \times 100\% \quad (2)$$

$$\text{Porosity} = \frac{w2 - w1}{w2 - w3} \times 100\% \quad (3)$$

where, $w1$: The dry specimen's weight (g), $w2$: The wet specimen's weight (g), $w3$: The submerged specimen's weight in water (g), and ρw: The density of water, which is (1 g/cm^3).

3.6.3. Compressive strength test

According to B.S. (1881-116) standard [26], a compressive strength test was conducted using (TONI PACT 3000, Germany) compressive strength test equipment. The loading speed was around 5.625 KN per second. The compressive strength was calculated by the following equation:

$$\sigma = P/A \quad (4)$$

where, σ is the compressive strength in (MPa), P is the maximum compressive load in (N), and A is the area of specimen in (mm^2).

3.6.4. Flexural strength recovery test

According to ASTM (C78) [27] standard, the bending strength was evaluated, and prior to four-point bending test, a notch was formed to a (3 mm) depth, and the download load was (0.2 MPa/s). After the test, the specimens were cured in the air

and left for another four weeks, and the bending strength can be calculated for (1st. R) as well as (2nd. R) by Eq. (5):

$$Fct = \frac{F*I}{d1*d2^2} \quad (5)$$

where, *Fct* is the flexural strength, expressed in MPa (N/mm^2), F is the ultimate load, expressed in (N), *I* is the span between the two supporting rollers, expressed in (mm), and (d1) as well as (d2) are the specimen's lateral dimensions (mm), and the identical prism samples from both combinations were examined once more after being healed for four weeks (2nd. R), using applicable equations to gauge the flexural strength recovery (6) [29]:

$$\eta\% = \frac{Fct2}{Fct1} \quad (6)$$

where, Fct1: The ultimate stress for the original specimen (1st. R), Fct2: The highest stress for the specimen beyond the healing (2nd. R), and $\eta\%$: The healing efficiency. The fracture seal was examined using a crack detection microscope on many occasions. The crack was photographed to measure its depth and width to calculate its percentage strength recovery over time. Where, the readings were taken, and the cracked prisms were indicated. The relative placements of the vascular network in the prism are displayed in Fig. 2.

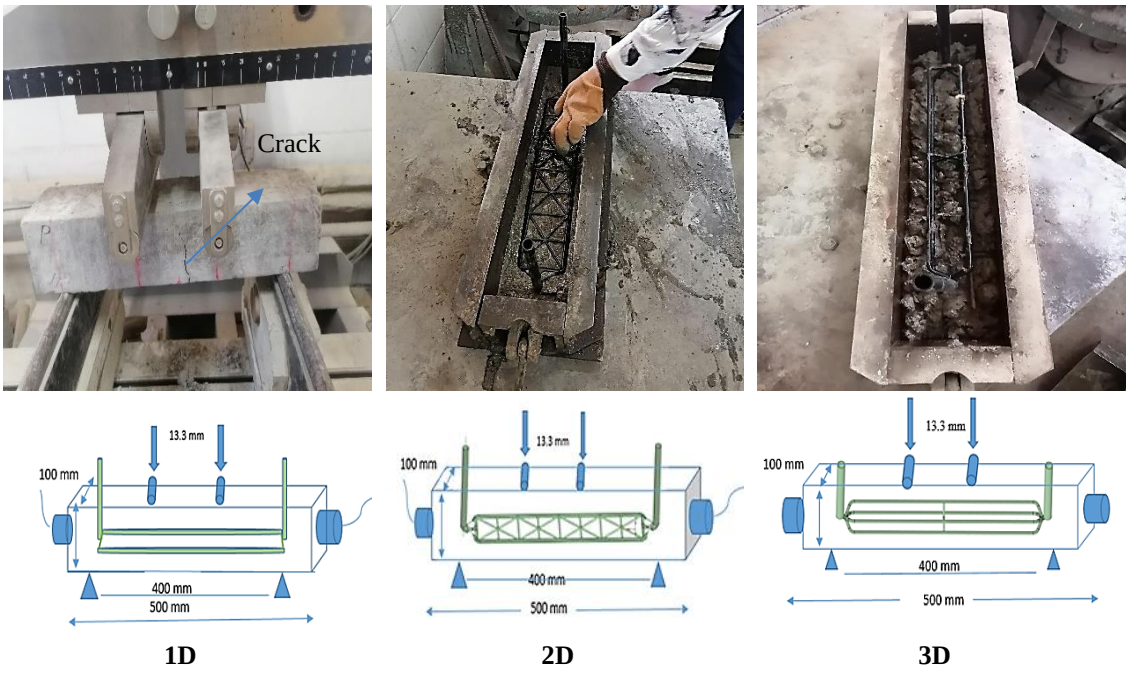

Fig. 2. Specimen showing an embedded (1D, 2D, and 3D) vascular network in prism.

3.6.5. Rapid chloride penetration test

Three cylindrical specimens with a diameter of 100 mm and a height of (200 mm) were prepared, and then, following the standard ASTM (C 1202) [30], they were formed into disc specimens having a diameter of 100 mm and a thickness of 50

mm. This was done to assess the resistance to chloride ion penetration. Following the application of 60 V for 6 hours, the anode and cathode were filled with 0.3 M NaOH and 3%NaCl, respectively. A schematic for this test system is portrayed in Fig. 3. The current passing value was monitored after the first current measurement at (30-min) intervals, and the overall passed charge was computed by Eq. (5).

$$Q = 900\,(I0 + 2I30 + 2I60 + \cdots + 2I300 + 2I330 + I360)$$

Fig. 3. The rapid chloride penetration test (RCPT) measurement device.

4. Result and Discussion

4.1. Scanning electron microscope (SEM)

SEM was used for the morphological study of fly ash (SA) nano-particles produced in a high-intensity ball milling. Figure 4 manifests that the FA has a uniform, spherical shape, which results in a rise in the surface area to enhance the pozzolanic reactivity, which makes the ball milling method suitable for obtaining regular spherical shapes and relative size ranges without affecting its spherical shape. This agrees with the researchers [31, 32].

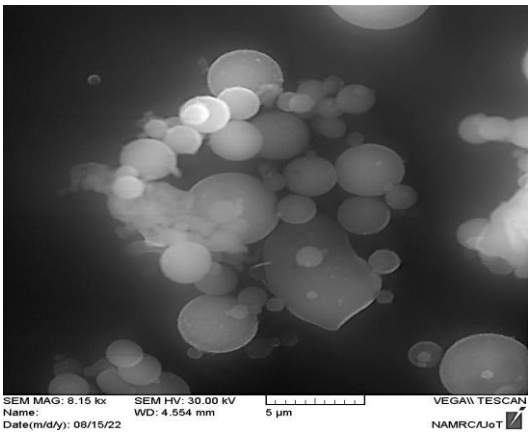

Fig. 4. The SEM micrograph image for Fly Ash Nano powder (NFA).

4.2. Particle size distribution (PSD) Results

The fly ash nanoparticles obtained from the planetary ball milling process were verified by the PSA instrument for evaluating the size of particles as well as the distribution of size through the procedure of milling. By the PSA, fly ash was successfully reduced to a (95.3 nm) particle size beyond the milling for (3) hours. It was seen that the close size distribution of the particle size distribution makes it very effective in promoting healing. The particle size distribution for the prepared FA nano-powder is displayed in Fig. 5.

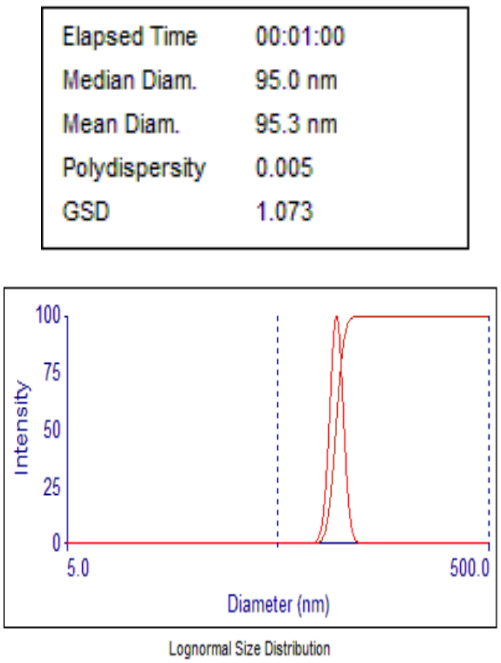

Fig. 5. Particle size distribution for the prepared FA Nano-powder.

4.3. Results of concrete supported (or reinforced) by PLA vascular tubes and network

4.3.1. Physical properties

When the concrete mixes are kept for 7 and 28 days, in relation to the experimental techniques to analyze the physical characteristics of the whole concrete mixes, the dry density raises with a rise in the healing agent content, as illustrated in Fig. 6.

High-strength dense gel (C-S-H), a product of the pozzolanic reaction, is created owing to the subsequent pozzolanic interactions of the particles of nano-fly ash (NFA) with the hydration product calcium hydroxide $Ca(OH)_2$ crystals. The transition zone's density was raised due to this process by filling in the voids left by the absence of material. The recent findings have demonstrated that, for all designs, an increase in the amount of healing agent lowered the porosity and water absorption in their values that agree with [33-35]. The highest rate of increase in density when adding 3D design with healing agent was 4% and 5.8% at 7 and 28

days, respectively, but the water absorption and porosity decreased at a rate (18.5%, 30%) and (14%, 36%) at 7 and 28 days, respectively.

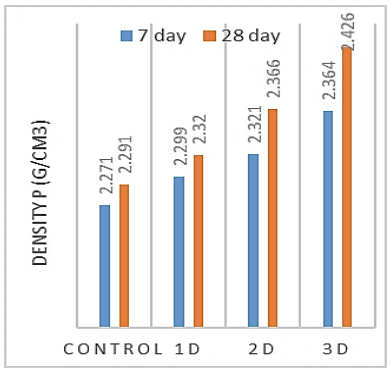

(a) Density

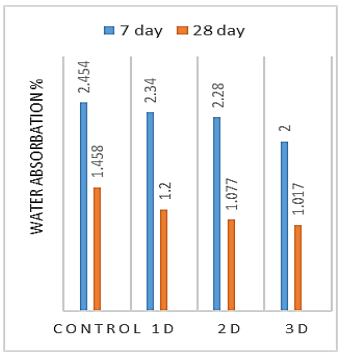

(b) Water absorption

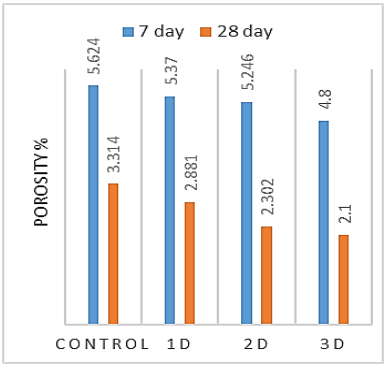

(c) Porosity

Fig. 6. Physical properties for concrete with different designs of vascular tube.

4.3.2. Compressive strength

The compressive strength test results are shown in Fig. 7 for all cube samples at 7 and 28 days of age. The findings are the averages for each of the three samples.

The compressive strength enhancement owing to the nano-fly ash (NFA) particles addition with sodium silicate can be ascribed to the high surface area of NFA, which can work as a nuclei location as well as encourage the hydration products creation, particularly the (C-S-H) gel. Since the PLA (hydrophobic material) tubes with a healing agent lead to the formation of a cohesive mix, and when the crack occurs, the healing material is released, leaving the cube in air curing for 28 days. Moreover, the compressive strength increased by capillary pore filling which corresponds well with previous studies [36-38]. The highest rate of increase in compressive strength, when adding 3D design with healing agent, was 25% and 30% at 7 and 28 days, correspondingly.

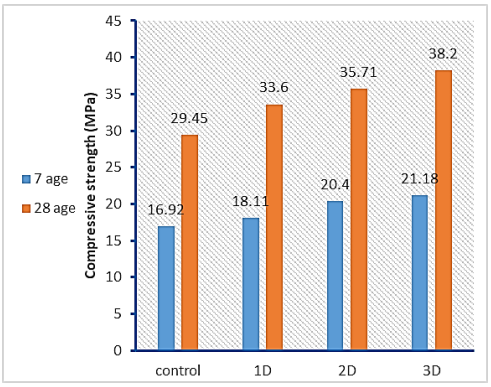

Fig. 7. Results of the compressive strength test.

4.3.3. Rapid chloride penetration resistance

The concrete specimens' test results for the chloride ion penetration resistance are elucidated in Fig. 8, which is significant in constructions made of plain concrete and measures the durability of the concrete. Whereas the higher value of RCPT showed the greater diffusion of concrete, the chloride ions existence has been observed to influence the concrete pavement's spalling beneath the pore solution's freezing point. It enhanced the rebar corrosion's saturation condition. The compressive strength [39], mineral admixtures like FA [40], aggregates, and approaches of curing, such as normal curing, autoclaving, steam curing, specimen temperature, size of pore, regional environmental conditions, test conditions, and sodium silicate [41, 42] are some of the variables that have an impact on the RCPT. When a healing agent was added to the concrete mix, the resistance to the penetration of chloride ions increased by 5%, 22%, and 32% for the (1D, 2D, and 3D) samples, respectively, in comparison to the reference sample. It is advised that a reasonable condition for concrete specimens has a total charge passing between 2000 and 4000°C.

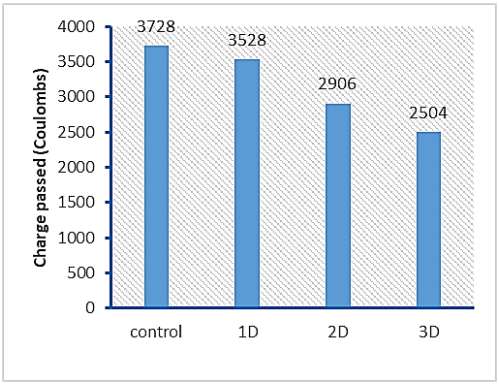

Fig. 8. Rapid chloride penetration resistance test results.

4.3.4. Flexural strength

The effectiveness of the vascular system's mechanical triggering and healing was assessed using loading recovery following the healing as observed in Fig. 9(a). The

materials entrenched with the prepared vascular networks (1D, 2D and 3D) underwent the 4-point bending tests to create cracks, as well as the outcomes are displayed in Fig. 10. An initial load (1st. R) applied to the plain cement beams aged 7 and 28 days demonstrated the least load response, at about (4.5 MPa) and (5.5 MPa), respectively. Comparing the specimens implanted with vascular networks with the control specimen, a greater force was needed for breaking the specimens, Fig. 10(a), possibly due to the physical activating or the tubes of PLA. Additionally, the vascular networks (1D, 2D and 3D) cracked with the higher strain applied, showing that the plastic tube reinforces the cement beams [43]. Equation (6) is used to assess the restoration of flexural strength. As shown in Fig. 9(b), the identical prism specimens from both combinations were re-evaluated after being healed for 28 days (2nd. R). According to the findings, the restored strength was 84% for the specimen with 3D and 43% for the control specimen. Comparing the results with the control specimen evinced that employing MC as a healing agent is effective, which is consistent with other researches [10, 44]. Compared with the systems of (1D) and (2D), the vascular system of (3D) was capable for blocking a larger region of the fracture. Due to the insufficient capillary force for pushing the healing agent upward as well as filling in the tip of crack, the systems of (1D) and (2D) could not provide healing agents in this location. And, due to their many supporting structures and lack of focus on a single tube, the 2D and 3D networks performed better under stress than the 1D structure.

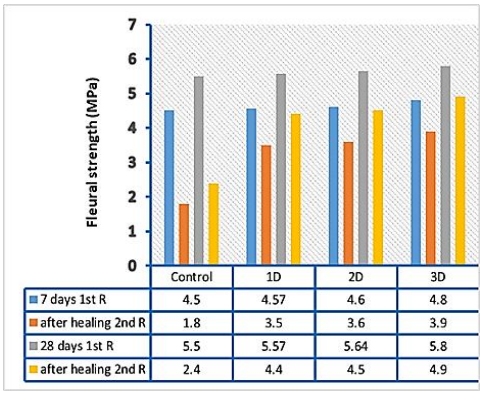

(a) Flexural strength recovery of all samples with a different design at 1st R and 2nd. R

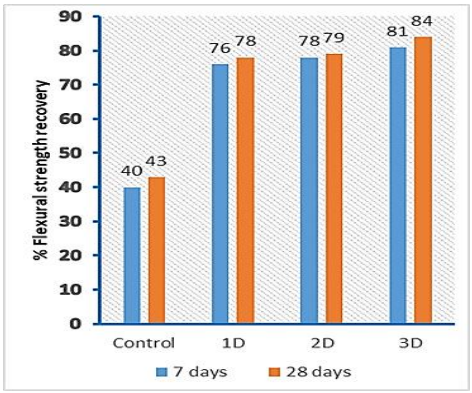

(b) Flexural strength percentage recovery of all samples

Fig. 9. Flexural strength for concrete with different designs of vascular tube.

4.3.5. Microstructure development analysis

Before and after self-healing, scanning electron microscopy was used to examine the broken surfaces, as shown in Figs. 10(a) and (b). On the cracked surfaces, there formed a layer of self-healing materials whose structure was distinct from the internal structure of cement paste seen in Figs. 10(c) and (d). This product layer expanded from the crack's surface to the centre. The analysis of microstructure was conducted. The control specimen formed mostly discrete crystals of CH and extended CSH gel from the residual hydrated cement particles as autonomous

healing products, filling only a tiny portion of the crack voids. The EDX investigation gave quantitative data for a more in-depth assessment of the chemical phases produced. The hydration degree of the C-S-H gels was obtained via the atomic ratio (Ca/Si). The lower the Ca/Si ratio, the more $Ca(OH)_2$ was consumed from the cement hydration **to** produce C-S-H linkages, which densified the matrix of concrete due to the nano filler effect. CH is formed even at an early curing age, prompting the pozzolanic reaction with NFA to create additional C-S-H binder gel. SEM and EDS were utilized in this work for evaluating the impact of the sodium silicate liquid with nano fly ash on the dimension of the microstructure [45-47]

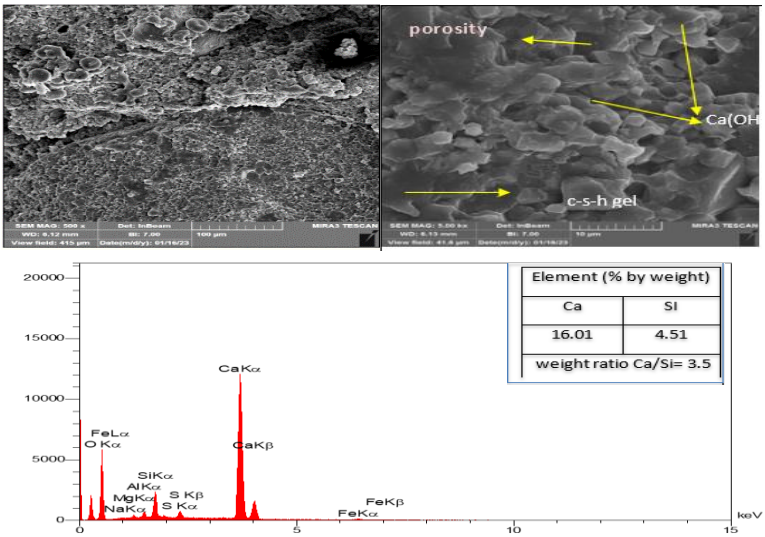

(a) SEM-EDS image of cementitious materials before self-healing at 7 days.

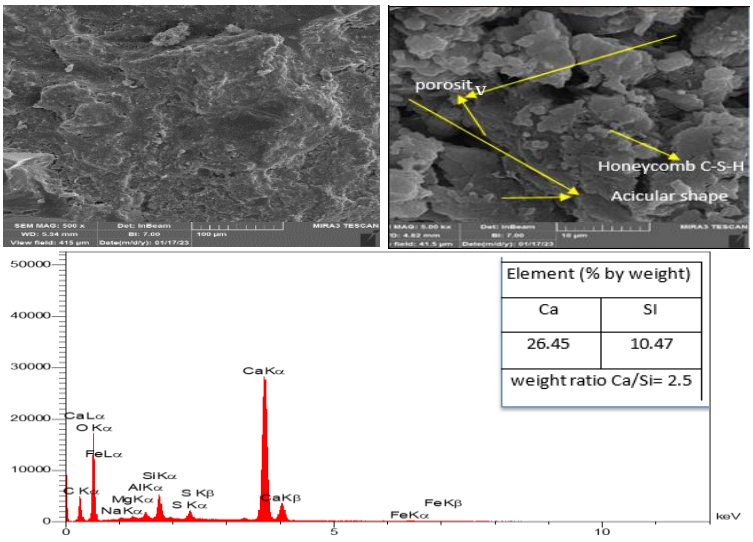

(b) SEM-EDS image of the cementitious materials before self-healing at 28 days.

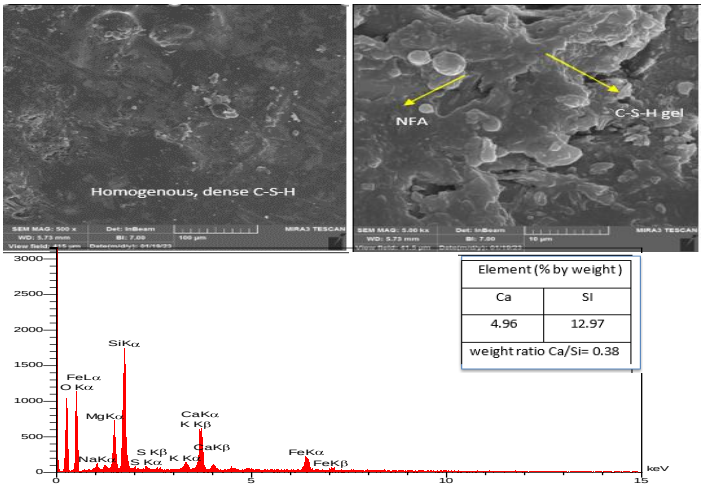

(c) SEM-EDS image of cementitious materials after self-healing with (sodium silicate holding nano fly ash powder) at 7days.

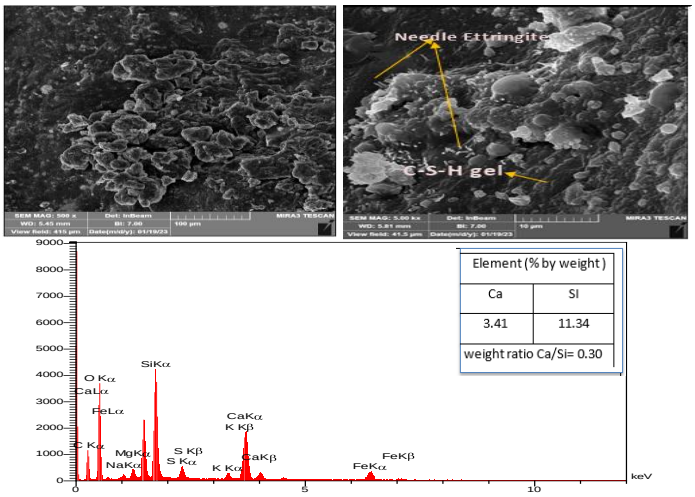

(d) SEM-EDS image of the cementitious materials after self-healing with (sodium silicate holding nano fly ash powder) at 28 days

Fig. 10. The SEM-EDS Images of cementitious materials before and after self-healing.

5. Conclusions

In conclusion, this study has shown that:

- The suggested self-healing system will be advantageous to include in concrete structures, such as underwater structures, bridges, and dams that are difficult to maintain and repair. Although the initial expenditures will be more significant since the damage is instantly repaired, the maintenance costs can be decreased, and the service life of the buildings may be maintained.

- The network's potential to promote multi-scale healing is improved because it may be employed with various healing agents and is reusable.
- Through a vascular system, the effective loading of powders enhanced the characteristics and sealing crack of the concrete beam.
- Mechanical repair was detected during the second loading cycle, demonstrating that the healing was verified.
- Because the healing agent was injected at several sites on the crack's surface, the 3D vascular system was capable to block more crack area, increasing the repaired surface, in comparison to the (1D) and (2D) systems.
- When the nano powder was added with liquid sodium silicate as a healing agent in concrete beams, the density and compressive resistance increased, resulting in greater pozzolan interaction and improved durability. The NFA minimized the permeability by filling the holes and cracks.

6. Future Perspectives

Monitoring mechanisms should be used to develop self-healing concrete, using optical fibers or piezoelectric transducers to create a sensor system that can identify the fractures and trigger the reservoir station's healing agent release. Future studies will focus on creating influential vascular healing networks and their implementation upon the concrete buildings.

Nomenclatures

1D	One-dimension vascular tube
2D	Two-dimension vascular tube
3D	Three-dimension vascular tube
A	The area of specimen, mm^2
$d1$ *and* $d2$	The lateral dimensions of specimen, mm
F	The ultimate load, N
F_{ct}	The flexural strength, MPa (N/mm^2)
f_{ct1}	The ultimate stress for the original specimen
f_{ct2}	The highest stress for the specimen beyond the healing
I	The span between the two supporting rollers, mm
NFA	Nano-Fly ash
P	The maximum compressive load, N
Q	Charge passed, coulombs
w/c	Water cement ratio
$w1$	The dry specimen's weight, g
$w2$	The wet specimen's weight, g

Greek Symbols

ρw	The density of water, 1 g/cm^3
η	The healing efficiency
σ	is the compressive strength, MPa

Abbreviations

ASTM	American Society for Testing and Materials
B.S	British Standard

EDS	energy Dispersive x-ray spectroscopy
FDM	Fused deposition modeling
PET	polyethylene terephthalate
PLA	Poly lactic acid
PVA	poly Vinyl alcohol
RCPT	Rapid chloride penetration test
SCM	Supplementary Cementitious materials
SEM	Scanning electron microscope
XRD	X- ray Diffraction

References

1. Formia, A.; Terranova, S.; Antonaci, P.; Pugno, N.M.; and Tulliani, J.M. (2015). Setup of extruded cementitious hollow tubes as containing/releasing devices in self-healing systems. *Materials*, 8(4), 1897-1923.
2. Šavija, B.; Zhang, H.; and Schlangen, E. (2017). Influence of microencapsulated phase change material (PCM) addition on (micro) mechanical properties of cement paste. *Materials*, 10(8), 863.
3. Dahesh, A.Z.; Othman, F.M.; and Abdul-Hamead, A.A. (2020). Improve mass concrete by controlling the crack sealing mechanism using microcapsules of zinc oxide. *Proceedings of the materials science forum*, 1002, 541-550
4. Huseien, G.F.; Shah, K.W.; and Sam, A.R.M. (2019). Sustainability of nanomaterials based self-healing concrete: An all-inclusive insight. *Journal of Building Engineering*, 23, 155-171.
5. Šavija, B. (2018). Smart crack control in concrete through use of phase change materials (PCMs): a review. *Materials*, 11(5), 654.
6. Aldea, C.M.; Song, W.J.; Popovics, J.S.; and Shah, S.P. (2000). Extent of healing of cracked normal strength concrete. *Journal of materials in civil engineering*, 12(1), 92-96.
7. Ribeiro de Souza, L. (2017). *Design and synthesis of microcapsules using microfluidics for autonomic self-healing in cementitious materials*. Doctoral dissertation, University of Cambridge.
8. Van Tittelboom, K.; De Belie, N.; Van Loo, D.; and Jacobs, P. (2011). Self-healing efficiency of cementitious materials containing tubular capsules filled with healing agent. *Cement and Concrete Composites*, 33(4), 497-505.
9. Minnebo, P., Thierens, G., De Valck, G., Van Tittelboom, K., De Belie, N., Van Hemelrijck, D.; and Tsangouri, E. (2017). A novel design of autonomously healed concrete: Towards a vascular healing network. *Materials*, 10(1), 49.
10. Li, Z., de Souza, L.R.; Litina, C.; Markaki, A.E.; and Al-Tabbaa, A. (2020). A novel biomimetic design of a 3D vascular structure for self-healing in cementitious materials using Murray's law. *Materials & Design*, 190, 108572.
11. Selvarajoo, T. (2020). *Characterisation of a vascular self-healing cementitious material system*. Doctoral dissertation, Cardiff University.
12. Siahkouhi, M.; Han, X.; Wang, M.; Manalo, A.; and Jing, G. (2023). Development and performance evaluation of self-healing concrete railway sleepers using different size PU tubes. *Engineering Structures*, 283, 115920.

13. Selvarajoo, T.; Davies, R.E.; Gardner, D.R.; Freeman, B.L.; and Jefferson, A. D. (2020). Characterisation of a vascular self-healing cementitious material system: flow and curing properties. *Construction and Building Materials*, 245, 118332.
14. Wan, Z.; Zhang, Y.; Xu, Y.; and Šavija, B. (2023). Self-healing cementitious composites with a hollow vascular network created using 3D-printed sacrificial templates. *Engineering Structures*, 289, 116282.
15. Tsangouri, E.; Van Loo, C.; Shields, Y.; De Belie, N.; Van Tittelboom, K.; and Aggelis, D.G. (2022). Reservoir-vascular tubes network for self-healing concrete: performance analysis by acoustic emission, digital image correlation and ultrasound velocity. *Applied Sciences*, 12(10), 4821.
16. De Nardi, C.; Freeman, B.L.; Gardner, D.; and Jefferson, T. (2023). Mechanical response and predictive modelling of vascular self-healing cementitious materials using novel healing agents. *Cement and Concrete Composites*, 142, 105143.
17. Alghamri, R.; Rengaraju, S.; and Al-Tabbaa, A. (2023). Large-scale laboratory trials of smart aggregates for self-healing in concrete under different curing regimes. *Cement and Concrete Composites*, 136, 104864.
18. Cruz J.; Hernandez S.; Trejo-Arroyo D.; Zarhri Z.; Z´arate-Medina J.; Jim´enez L.F.; and Gurrola M. (2022) *Materials Research Express*, 9, 025506
19. Sajjadi, S.; and Madandoust, R. (2021). Evaluation of self-healing performance of concrete containing fly ash and fibres. *Australian Journal of Structural Engineering*, 22(3), 177-190.
20. Anglani, G.; Antonaci, P.; Gonzales, S.I.C.; Paganelli, G.; and Tulliani, J.M. (2019, June). 3D printed capsules for self-healing concrete applications. *Proceedings of the 10th International Conference on Fracture Mechanics of Concrete and Concrete Structures (FraMCoS-X), Bayonne, France*, 24-26.
21. IQS 5/1984, (1984). Portland cement central organization for standardization and quality control Iraq Tech. rep. Central Organization for Standardization and Quality Control Baghdad, IQ (in Arabic).
22. ASTM, C. (2004). C150-04, Standard specification for Portland cement. West Conshohocken: ASTM International, 4.1, 1–8.
23. IQS 45/1980, (1980). Aggregates from natural sources for concrete and building construction Tech. rep. Central Organization for Standardization and Quality Control Baghdad, IQ (in Arabic).
24. ASTM, C. (2003). C33-2003, Standard specification for concrete aggregates. West Conshohocken: ASTM International, 4.2, 1–11.
25. ASTM, C. (2015). C 618, Standard specification for coal fly ash and raw or calcined natural pozzolan for use in concrete. West Conshohocken: ASTM International.
26. Standard, B. (1983). 1881- Part 116 testing concrete: Method for determination of compressive strength of concrete cubes.
27. ASTM, C. (2016). C78-16, Standard test method for flexural strength of concrete (Using simple beam with third-point loading). West Conshohocken: ASTM International.

28. ASTM, C. (1997). C642-1997, Standard test method for density, absorption, and voids in hardened concrete. ASTM Designation.
29. Minnebo, P.; Thierens, G.; De Valck, G.; Van Tittelboom, K.; De Belie, N., Van Hemelrijck, D.; and Tsangouri, E. (2017). A novel design of autonomously healed concrete: Towards a vascular healing network. *Materials*, 10(1), 49.
30. ASTM, C. (2019). C1202 Standard test method for electrical indication of concrete's ability to resist chloride ion penetration. American Society for Testing Materials, West Conshohocken: ASTM International.
31. Kaur, M.; Singh, J.; and Kaur, M. (2018). Microstructure and strength development of fly ash-based geopolymer mortar: Role of nano-metakaolin. *Construction and Building Materials*, 190, 672-679.
32. Harihanandh, M.; Viswanathan, K.E.; and Krishnaraja, A.R. (2021). Comparative study on chemical and morphology properties of nano fly ash in concrete. *Materials Today: Proceedings*, 45, 3132-3136.
33. Alobaidi, Y.M.; Hilal, N.N.; and Faraj, R.H. (2021). An experimental investigation on the nano-fly ash preparation and its effects on the performance of self-compacting concrete at normal and elevated temperatures. *Nanotechnology for Environmental Engineering*, 6, 1-13.
34. Alam, M.A.; and Al Riyami, K. (2018). Shear strengthening of reinforced concrete beam using natural fibre reinforced polymer laminates. *Construction and Building Materials*, 162, 683-696.
35. Abdul-hamead, A.A.; Othman, F.M.; and Abdullah, D.M. (2019, July). Smart cement modified with nano fly ash and micro fiber for oil well applications. *IOP Conference Series: Materials Science and Engineering*, 579, 012008.
36. Wang, X.; Qiao, H.; Zhang, Z.; Tang, S.; Liu, S.; Niu, M.; and Li, G. (2021). Effect of fly ash on the self-healing capability of cementitious materials with crystalline admixture under different conditions. *AIP Advances*, 11(7), 075018.
37. Patil, A.Y.; Banapurmath, N.R.; EP, S.; Chitawadagi, M.V.; Khan, T.Y.; Badruddin, I.A.; and Kamangar, S. (2020). Multi-scale study on mechanical property and strength of new green sand (Poly Lactic Acid) as replacement of fine aggregate in concrete mix. *Symmetry*, 12(11), 1823.
38. Abdul-hamead, A.A.; Othman, F.M.; and Hmeed, N.A. (2018). The effect of nano fly ash on properties of cement mortar. *AIP Conference Proceedings*, 2045(1), 020011.
39. Mohr, P.; Hansen, W.; Jensen, E.; and Pane, I. (2000). Transport properties of concrete pavements with excellent long-term in-service performance. *Cement and Concrete Research*, 30(12), 1903-1910.
40. Moffatt, E.G.; Thomas, M.D.; and Fahim, A. (2017). Performance of high-volume fly ash concrete in marine environment. *Cement and Concrete Research*, 102, 127-135.
41. Rajhans, P.; Gupta, P.K.; Kumar, R.R.; Panda, S.K.; and Nayak, S. (2019). EMV mix design method for preparing sustainable self compacting recycled aggregate concrete subjected to chloride environment. *Construction and Building Materials*, 199, 705-716.
42. Rajhans, P.; Chand, G.; Kisku, N.; Panda, S.K.; and Nayak, S. (2019). Proposed mix design method for producing sustainable self compacting heat

cured recycled aggregate concrete and its microstructural investigation. *Construction and Building Materials*, 218, 568-581.

43. Kim, B.; and Han, Y.J. (2018). Flexural performance of transparent plastic bar reinforced concrete. *Applied Sciences*, 8(3), 325.
44. Sallal, H.A.; Abdul-Hamead, A.A.; and Othman, F.M. (2020). Effect of nano powder (Al_2O_3-CaO) addition on the mechanical properties of the polymer blend matrix composite. *Defence Technology*, 16(2), 425-431.
45. Cheah, C.B.; Tiong, L.L.; Ng, E.P.; and Oo, C.W. (2019). The engineering performance of concrete containing high volume of ground granulated blast furnace slag and pulverized fly ash with polycarboxylate-based superplasticizer. *Construction and Building Materials*, 202, 909-921.
46. Kunther, W.; Ferreiro, S.; and Skibsted, J. (2017). Influence of the Ca/Si ratio on the compressive strength of cementitious calcium–silicate–hydrate binders. *Journal of Materials Chemistry A*, 5(33), 17401-17412.
47. Cheah, C.B.; Chow, W.K.; Oo, C.W.; and Leow, K.H. (2020). The influence of type and combination of polycarboxylate ether superplasticizer on the mechanical properties and microstructure of slag-silica fume ternary blended self-consolidating concrete. *Journal of Building Engineering*, 31, 101412.